Applied Catalysis B: Environmental 162 (2015) 268–274

Contents lists available at ScienceDirect

Applied Catalysis B: Environmental

journal homepage: www.elsevier.com/locate/apcatb

In situ fabrication of Mn_3O_4 decorated graphene oxide as a synergistic catalyst for degradation of methylene blue

Yuqian Li[a], Jiangying Qu[a,c,*], Feng Gao[a,c], Siyuan Lv[a], Lin Shi[a], Chunxiang He[a,*], Jingchang Sun[b]

[a] Faculty of Chemistry and Chemical Engineering, Liaoning Normal University, Dalian 116029, Liaoning, China
[b] School of Physics and Electronic Technology, Liaoning Normal University, Dalian 116029, Liaoning, China
[c] Carbon Research Laboratory, Center for Nano Materials and Science, School of Chemical Engineering, State Key Lab of Fine Chemicals, Dalian University of Technology, Dalian 116024, Liaoning, China

ARTICLE INFO

Article history:
Received 28 April 2014
Received in revised form 29 June 2014
Accepted 30 June 2014
Available online 8 July 2014

Keywords:
Graphene oxide
Mn_3O_4
Methylene blue
Degradation
Green method

ABSTRACT

Herein we report a one-step approach to the highly efficient synthesis of graphene oxide/Mn_3O_4 (GO/Mn_3O_4) hybrids with superior catalytic activities for decomposition of methylene blue (MB) in water. This method exploits the pristine graphene oxide/manganese sulfate (GO/$MnSO_4$) suspension produced by the modified Hummers method as the raw materials, in which GO/$MnSO_4$ has been *in situ* converted into GO/Mn_3O_4 hybrid in combination with KOH and air. This atom-economic reaction produces only K_2SO_4 crystal as the by-product which meets the standard of green chemistry. For catalystic degradation of MB dye at room temperature, the as-prepared GO/Mn_3O_4 catalysts result in a significant enhancement in the reaction rate compared to that of the bare Mn_3O_4 particles with the assistance of H_2O_2. Typically, 50 mL of MB (50 mg L^{-1}) can be 100% decolorized and 77% mineralized with 10 mg of the GO/Mn_3O_4 hybrid. Such excellent catalytic performance of the GO/Mn_3O_4 hybrid is mainly attributed to the synergistic effects of GO, Mn_3O_4, H_2O_2 and MB molecules. Based on the hydroxyl radical experiments, the catalytic activity of GO/Mn_3O_4 hybrids for degradation of MB is closely related with the amount of the reactive •OH species generated from H_2O_2.

1. Introduction

The increasing amounts of wastewater containing toxic and hazardous organic compounds are generated by various industrial processes, which have caused severe problems to the environment. Tremendous efforts have been dedicated to alleviate the deterioration in water body around the world. Manganese oxide (MnO_x, $x = 2$, 3/4), a non-toxicity and low cost metal oxide has been widely used as a catalyst for oxidation of organic compounds. However, MnO_x particles often suffer from aggregation as well as poor stability, which devastate their catalytic efficiency [1–3]. The combination of MnO_x ($x = 1$, 2, 4/3) and carbon materials should be an alternative way to address above problems. Particularly, graphene with good stability, large surface area and unique electronic property provides a promising candidate [4–6]. Recently, graphene oxide (GO) produced by modified Hummers method has been widely selected as the precursor to produce graphene/MnO_x composites [7–11]. Typically, GO from Hummers method involves formation of a mixture suspension containing GO, K_2SO_4, $MnSO_4$ and H_2SO_4 by intercalation and oxidation of graphite with H_2SO_4 and $KMnO_4$, followed by a fussy process to separate these compounds from GO. This separation process is time consuming and results in the waste of K_2SO_4, $MnSO_4$ and H_2SO_4. Inspired by the high content of Mn^{2+} in the mixture before separation, a highly atom-economic method has been suggested to produce reduced graphene oxide/MnO_2 from the mixture instead of GO suspension [12]. The obtained materials exhibited ultrafast decomposition of methylene blue (MB) dye at 50 °C in the presence of H_2O_2. In spite of our efforts, a large amount of toxic and highly corrosive H_2SO_4 generated during the synthesis process still represents a menace to the environment. Furthermore, the MB decolorization degree of the RGO/MnO_2 was 100% in 5 min at 50 °C but only 86% in 200 min at room temperature. The low catalytic performance of the RGO/MnO_2 at room temperature was partly ascribed to the irreversible agglomeration of graphene because of its hydrophobic nature in water.

GO, one of the most important derivative of graphene, consists of a hexagonal ring-based carbon network with both

* Corresponding authors at: Liaoning Normal University, Faculty of Chemistry and Chemical Engineering, Dalian, Liaoning 116029, China. Tel.: +86 411 82158329.
E-mail addresses: qujy@lnnu.edu.cn (J. Qu), hcx0224@163.com (C. He).

http://dx.doi.org/10.1016/j.apcatb.2014.06.058
0926-3373/

sp^2- and sp^3-hybridized carbon atoms. This carbon material has multiple oxygen-containing functional groups, such as hydroxyls and carboxylic acid groups bearing on its basal planes and edges. Previous study has showed that GO sheets are highly negatively charged when dispersed in water, apparently as a result of ionization of the carboxylic acid and phenolic hydroxyl groups [13,14]. Thus electrostatic repulsions between GO sheets eventually facilitate their dispersion in water. Furthermore, the negatively charged surfaces of GO are benefit to remove cationic dyes by electrostatic attraction when it is used as an adsorbent [15]. Except for the charged surfaces, GO is a layered material that can be intercalated or exfoliated by small molecules. These exfoliated GO sheets with suitable surface areas can be used as ideal support materials to load metal or metal oxide particles, resulting in the composites to be good catalysts for the removal of environmental pollutants [7,16–24]. Recently, several groups reported on the synthesis of GO/TiO_2 composites and their application in photocatalytic degradation of various dyes [18,21,25,26]. For instance, Shi et al. demonstrated that GO/Co_3O_4 composite was a synergistic catalyst to degrade Orange II by advanced oxidation technology based on sulfate radicals [27]. GO/CdS composites also showed high efficiency in photodegradation of various water pollutants under visible light irradiation [20]. These studies reveal that the GO may be promising support materials to separate pollutants from wastewater. However, the application of GO as a catalyst support is still scarce, and the synergistic effects between GO, catalyst and dye pollutants are not studied in detail.

Herein, we present a one-step method to fabricate GO/Mn_3O_4 composites which can highly effective decomposition of MB with the assistance of H_2O_2. GO/$MnSO_4$ suspension produced by the modified Hummers method has been converted into GO/Mn_3O_4 hybrid *in situ* in combination with KOH and air. Compared with our previous report about RGO/MnO_2 catalysts [12], we get more advantages in this work as followed: (1) toxic and highly corrosive H_2SO_4 produced from Hummers method is eliminated during the atom-economic synthesis of GO/Mn_3O_4 composites; (2) the chemical reduction of GO into graphene is avoided; (3) Mn_3O_4 nanoparticles are distributed on GO sheets to avoid the restacking of GO as well as the agglomeration of Mn_3O_4; (4) good hydrophilicity of GO toward aqueous solution and electrostatic attractions existed in between GO and MB are favorable to the catalytic reaction; (5) MB dye is decomposed at room temperature; (6) excellent contact between Mn_3O_4 nanoparticles and GO sheets enhances the durability of GO/Mn_3O_4 composites. As expected, the resulting GO/Mn_3O_4 composites exhibit higher catalytic efficiency than that of bare Mn_3O_4 when MB dye is used as a test probe.

2. Experimental

2.1. Synthesis of GO/Mn_3O_4 composites

The pristine GO/$MnSO_4$ suspension was synthesized from natural graphite powder based on a modified Hummers method according to our previous work [28]. Typically, 10 mL of the homogeneous GO/$MnSO_4$ suspension was diluted to 100 mL and then sonicated for 1 h. An aqueous solution of KOH (2 mol L^{-1}) was added dropwise into the above solution under bubbling air and stirring until the pH value of solution reached 12. After exposure in air for 6 h, the sediment composed of GO/Mn_3O_4 was harvested by several rinse–centrifugation cycles with deionized water until the solution became neutral. The collected precipitate was fully dried at 80 °C overnight to get GO/Mn_3O_4 composites.

Composites with different mass percentages of Mn_3O_4 were synthesized as below. Two test tubes, each containing 10 mL of homogeneous pristine GO/$MnSO_4$ suspension, were labeled as A and B. The suspension in tube A was centrifuged at 8000 rpm for 10 min to spin down GO as precipitate and to get supernatant liquid (including $MnSO_4$, H_2SO_4, K_2SO_4). And diverse amount of supernatant liquid in tube A was transferred to tube B. So the GO/$MnSO_4$ suspensions with the different mass ratios of GO to $MnSO_4$ were obtained. The following processes were similar to those of GO/Mn_3O_4 synthesis. The as-synthesized samples were denoted as GO/Mn_3O_4-*X*, where *X* represented the mass percentages of Mn_3O_4 in GO/Mn_3O_4 composites. For comparison, bare Mn_3O_4 particles or GO was synthesized by a similar procedure in the absence of GO or Mn_3O_4. Furthermore, GO/Mn_3O_4-74 was reduced by glucose to produce RGO/Mn_3O_4 according to the reference [12].

2.2. Test of the catalytic activity

The catalytic performances of as-synthesized GO/Mn_3O_4 composites were evaluated with GO and Mn_3O_4 particles as the reference. The catalytic reaction was performed in a 100 mL glass beaker containing 50 mL of MB dye solution (50 mg L^{-1}), 10 mg of catalysts and 10 mL of 30 wt% H_2O_2 solution. The mixture was stirred at room temperature. For a given time interval, 4 mL of the mixture solution was centrifuged at 10,000 rpm for 10 min to get a supernatant liquid, leaving the catalysts as the precipitate. The dye concentration was determined by the peak intensity at 664 nm by UV–vis spectroscopy. Furthermore, in the stability tests of GO/Mn_3O_4-74 composite, the catalyst was gathered after completion of the reaction, washed, dried, and reused in a fresh solution of MB and H_2O_2. After reaction, the sample, named as GO/Mn_3O_4-74-used, was gathered for further characterization.

2.3. Analysis of hydroxyl radical (•OH)

The measurement of •OH was carried out by a similar procedure described in Ref. [29,30]. Typically, 10 mg of a certain kind of as-synthesized catalysts was dispersed in a 50 mL aqueous solution involved 5×10^{-4} mol L^{-1} of terephthalic acid (TA) and 2×10^{-3} mol L^{-1} of NaOH. Subsequently, 10 mL of 30 wt% H_2O_2 solution was added. The reactions were performed under continuous stirring at room temperature. A sample (5 mL) was removed in 5 min interval, and the catalyst was separated from the solution with centrifugation. The remaining clear liquid was used for fluorescence spectrum measurements. PL spectra of generated 2-hydroxyterephthalic acid were measured at 446 nm excited by 325 nm light.

The morphologies and structures of the as-obtained products were examined using transmission electron microscopy (TEM, Philips Tecnai G2 20), field emission scanning electron microscopy (SEM, Hitachi Ltd SU8010), powder X-ray diffraction (XRD, Rigaku D/max-2500 diffractometer with Cu *K*α radiation), Raman spectroscopy (JY Lab-Ram HR800), X-ray photoelectron spectroscopy (XPS, Thermo VG Scientific Sigma Probe spectrometer), thermogravimetric analyses (TGA, Perkin-Elmer Diamond TG analyzer), UV–vis spectroscopy (Shimazu UV-3150 spectroscope), ion chromatograph (Shimadzu, LC-10ADsp Ion Chromatograph), inductively coupled plasma emission spectroscopy (ICP, Perkin Elmer, Optima 2000DV) and photoluminescence spectra (PL, Hitachi, F-7000 fluorescence spectrophotomete), H_2 temperature-programed reduction (H_2-TPR, Mircromeritics, ChemiSorb 2720). The Brunauer–Emmett–Teller (BET) surface area of as-synthesized samples was determined by physisorption of N_2 at 77 K using a Micromeritics ASAP 2020 analyzer.

3. Results and discussion

A highly economical method was presented to fabricate GO/Mn_3O_4 hybrids for oxidative decomposition of MB dye (illustrated in Fig. 1). Pristine GO/$MnSO_4$ suspension (including GO, $MnSO_4$, H_2SO_4, K_2SO_4) produced by the modified Hummers method was directly used as the raw materials, which were *in situ* converted into GO/Mn_3O_4 hybrids by air oxidation in the presence of KOH following the stoichiometric reaction: $6Mn^{2+} + 12OH^- + O_2 = 2Mn_3O_4 + 6H_2O$. The resulting GO/$Mn_3O_4$ hybrids were employed as catalysts for decomposition of MB dye in the presence of H_2O_2 while K_2SO_4 crystal as the only byproduct was recycled.

XRD patterns of GO/Mn_3O_4-74 composite before and after catalytic oxidation of MB were shown in Fig. 2a with that of bare Mn_3O_4 particles and GO as the references. The diffraction patterns of both GO/Mn_3O_4-74 composite and bare Mn_3O_4 particles show intense peaks corresponding to (1 1 2), (1 0 3), (2 1 1), (2 2 0), (1 0 5), (3 2 1), (2 2 4) and (4 0 0) planes, which match well with previous reported hausmannite structure of Mn_3O_4 (JCPDS no. 24-0734) [31,32]. Furthermore, the peak at around 11° of GO/Mn_3O_4-74 composite can be indexed to (0 0 1) plane of GO, and its intensity is weaker compared with that of bare GO due to the presence of Mn_3O_4 [28].

Raman spectra further provided complementary structural information to XRD. The typical Raman spectra taken from different regions of the bare Mn_3O_4, GO particles and GO/Mn_3O_4-74 composite are shown in Fig. 2b. The GO has Raman-active bands in-phase vibration of the graphite lattice (G band) at 1592 cm^{-1} and the disorder band caused by oxidation process of the graphite edges (D band) at approximately 1342 cm^{-1} due to attachment of oxygen-containing functional groups [31,33]. The intensity ratio between the D and G bands (I_D/I_G) of GO (1.1) is the same to that of GO/Mn_3O_4-74 composite (1.1) due to the presence of abundant oxygen-containing groups, indicating that the functional groups of GO remains after formation of the hybrid structure. Furthermore, the minor peak of Raman scattering at 646 cm^{-1} associated with hausmannite phase of Mn_3O_4 [33,34] can be observed in GO/Mn_3O_4-74 composite and in bare Mn_3O_4 particles. Raman and XRD analyses confirm the coexistence of both GO and Mn_3O_4 in the as-prepared composite.

The chemical bonding states in GO/Mn_3O_4-74, GO/Mn_3O_4-74-used composites and GO were analyzed by XPS measurements, and the fitted data were shown in Fig. 3. Compared with the XPS survey spectrum of GO, the spectrum of the GO/Mn_3O_4-74 exhibits not only O 1s and C 1s peaks but two peaks of Mn 2p states, illustrating the presence of Mn species in GO/Mn_3O_4-74 composite [33,35]. As shown in Fig. 3b, the XPS spectra for the Mn 2p of the composite exhibit two peaks at 641.2 and 652.8 eV, corresponding to the Mn $2p_{3/2}$ and Mn $2p_{1/2}$ states of Mn_3O_4, respectively. It is observed that there is an energy separation of 11.6 eV between the Mn $2p_{1/2}$ and Mn $2p_{3/2}$ peaks, which is in agreement with an earlier report on Mn_3O_4 [35]. The C 1s deconvolution spectrum of GO/Mn_3O_4-74 composite is analyzed by curve fitting, shown in Fig. 3c. The spectrum reveals the presence of four components of the carbon bond: C—C/C=C (284.6 eV), C—O (286.6 eV), C=O (288.3 eV) and O—C=O (289.0 eV), which are in good agreement with the literature values on GO [7,33]. In the case of oxygen (Fig. 3d), three different peaks centered at 529.2, 531.2, 532.8 eV are corresponding to Mn—O—Mn, Mn—O—H and C—O/C=O in the GO/Mn_3O_4-74 composite, respectively [7]. The presence of Mn—O—H indicates the existence of strong interaction between Mn_3O_4 and GO. XPS analyses are in good agreement with the XRD and Raman results.

Thermal stability and quantified composition of the GO/Mn_3O_4 composites were analyzed by TGA. The experiments were performed from room temperature to 770 °C in air flow at a heating rate of 10 °C min^{-1}. As shown in Fig. 4a, GO/Mn_3O_4-74 composite shows a three-step weight loss: (1) weight loss below 100 °C is attributed to dehydration of physically adsorbed water molecules; (2) weight loss is observed at around 200 °C which has been previously assigned to the removal of oxygenate groups on the surfaces of GO; (3) the loss of weight above 300 °C occurs due to the removal of carbon sketch by burning of GO [22]. At last, Mn_3O_4 with the weight percent of 74% is left at 770 °C when GO is burned up (evidenced by XRD analysis in Fig. 4b). Accordingly, the mass percentages of Mn_3O_4 in GO/Mn_3O_4 composite can be derived to be 74%. By varying the quantity of supernatant liquid of pristine GO/$MnSO_4$ suspension in the reaction mixture (shown in Section 2.1), GO/Mn_3O_4 composites with different Mn_3O_4 loadings can be further prepared. For instance, the mass percentage of Mn_3O_4 in GO/Mn_3O_4 composites is estimated as 84% and 62%.

The SEM and TEM images of GO/Mn_3O_4-74 composite and bare Mn_3O_4 particles were shown in Fig. 5a–c. GO features large and thin nanosheets with Mn_3O_4 nanoparticles of about 30–50 nm uniformly distributed on its surface (Fig. 5a and b). The morphology of Mn_3O_4 particles changes a lot in the absence of GO, which seriously aggregates together into massive particles (Fig. 5c). Such results indicate that the present GO can prevent the aggregation of Mn_3O_4 nanoparticles efficiently. This observation is attributed to the fact that the abundant oxygen-containing functional groups, such as hydroxyl and carboxyl groups on the surface of GO can absorb or anchor Mn^{2+}, then limit Mn_3O_4 nanoparticles to agglomerate [31,36–39].

The application of as-synthesized GO/Mn_3O_4 composites was studied for decomposition of MB with the assistance of H_2O_2 at room temperature. At a certain reaction interval, the UV–vis spectroscopy of the dye in aqueous solution was measured after catalyzed by GO/Mn_3O_4-74 composite. As shown in Fig. 6a, two characteristic peaks (614 and 664 nm) are observed from the starting solution of MB which is attributed to typical MB peaks [2,40]. The absorption peak diminishes with prolonged time, and the solution turns colorless gradually within 200 min (shown in the inset of Fig. 6a). To clarify the performance of the catalysts, a systematic investigation is carried out. The relationship between MB decoloration degree and reaction time for different samples is shown in Fig. 6b. The results show that about 50, 22 and 6%

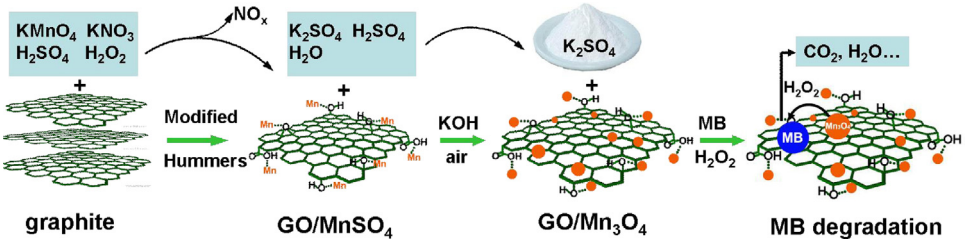

Fig. 1. Schematic illustration of green synthesis of GO/Mn_3O_4 hybrids by means of the modified Hummers method and air oxidation as well as their application for decomposition of MB.

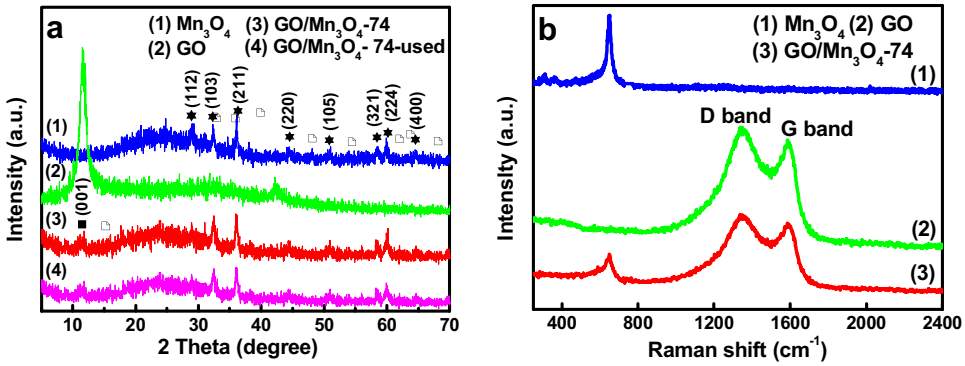

Fig. 2. (a) XRD patterns and (b) Raman spectra of bare Mn_3O_4, GO, GO/Mn_3O_4-74 and GO/Mn_3O_4-74-used composites.

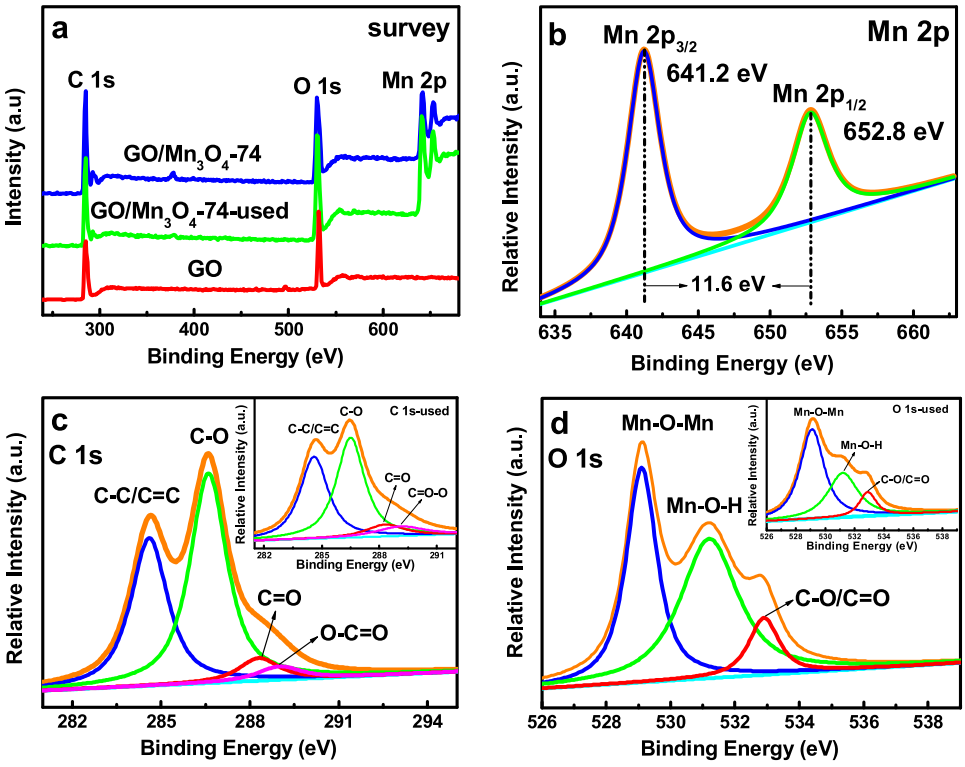

Fig. 3. XPS spectra of GO/Mn_3O_4-74, GO/Mn_3O_4-74-used composites and GO: (a) the survey scan; ((b)–(d)) Mn 2p region, O 1s region and C 1s region of GO/Mn_3O_4-74 composite, the insets are the O 1s region and C 1s region of GO/Mn_3O_4-74-used composite.

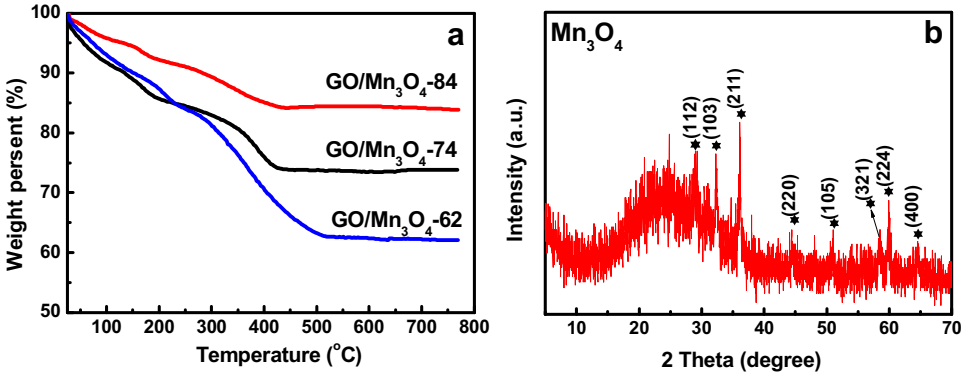

Fig. 4. (a) TGA of GO/Mn_3O_4 composites with different Mn_3O_4 loadings and (b) XRD pattern of the corresponding product (Mn_3O_4) after thermal treatment of GO/Mn_3O_4-74 at 770 °C in air atmosphere.

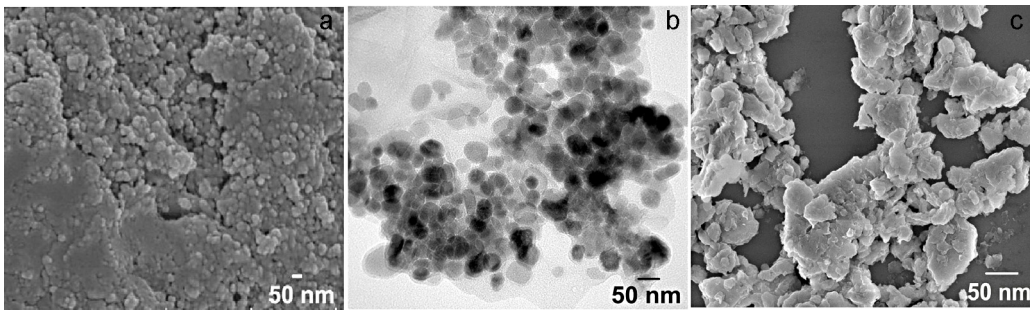

Fig. 5. ((a) and (b)) SEM and TEM images of GO/Mn_3O_4-74 composite, (c) SEM image of bare Mn_3O_4 particles in the absence of GO.

MB are, respectively, absorbed by GO/Mn_3O_4-74 composite, GO and bare Mn_3O_4 particles in the absence of H_2O_2. In the absence of catalyst (only MB and H_2O_2), the degree of MB decolorization is about 8%, showing the slow oxidative decomposition of MB for H_2O_2. In conclusion, the coexistence of GO/Mn_3O_4 and H_2O_2 plays an important role on efficient decomposition of MB dye from water. Furthermore, the effect of mass ratio of Mn_3O_4 to GO on the decomposition of MB with the assistance of H_2O_2 is also investigated. It can be seen that GO/Mn_3O_4 composites show gradually increased degree of MB decolorization from 88 to 100% with the increasing content of Mn_3O_4 from 62 to 74 wt% within 200 min, respectively. Further increase of Mn_3O_4 content to 84 wt% leads to only 95% MB decolorization under the same condition. Hence, the catalytic activity of as-prepared samples depends on the suitable ratio of Mn_3O_4 to GO. GO/Mn_3O_4-74 composite demonstrates the highest catalytic activity of 100% for decomposition of MB dye, which is much higher than that of each individual component (GO for 25% and bare Mn_3O_4 for 76% in 200 min). For comparison, the MB decolorization degree is about 91% in 200 min for GO/Mn_3O_4-mixture composite (mechanically mixed composite with a mass ratio 74/26 of Mn_3O_4 to GO). Accordingly, the degree of MB decolorization for these samples decreases in the following order: GO/Mn_3O_4-74 > GO/Mn_3O_4-mixture > bare Mn_3O_4 > GO.

The excellent catalytic activity of GO/Mn_3O_4-74 hybrid probably originates from positive synergistic effects between Mn_3O_4 and GO. The synergistic effects here may relate with mechanical interactions and chemical binding [36]. First, the anchoring Mn_3O_4 nanoparticles onto the GO sheets is proposed as *in situ* intercalation and adsorption of Mn^{2+} into the layered GO sheets followed by the nucleation and growth of Mn_3O_4 nanoparticles. A sandwich architecture between GO sheets and Mn_3O_4 particles through mechanical interaction has been formed based on SEM and TEM observations, which is also speculated to avoid the agglomeration of Mn_3O_4 (Supporting information Fig. S1a). Thus GO/Mn_3O_4-74 composite possesses a higher degree of MB decolorization as compared to bare Mn_3O_4. Second, according

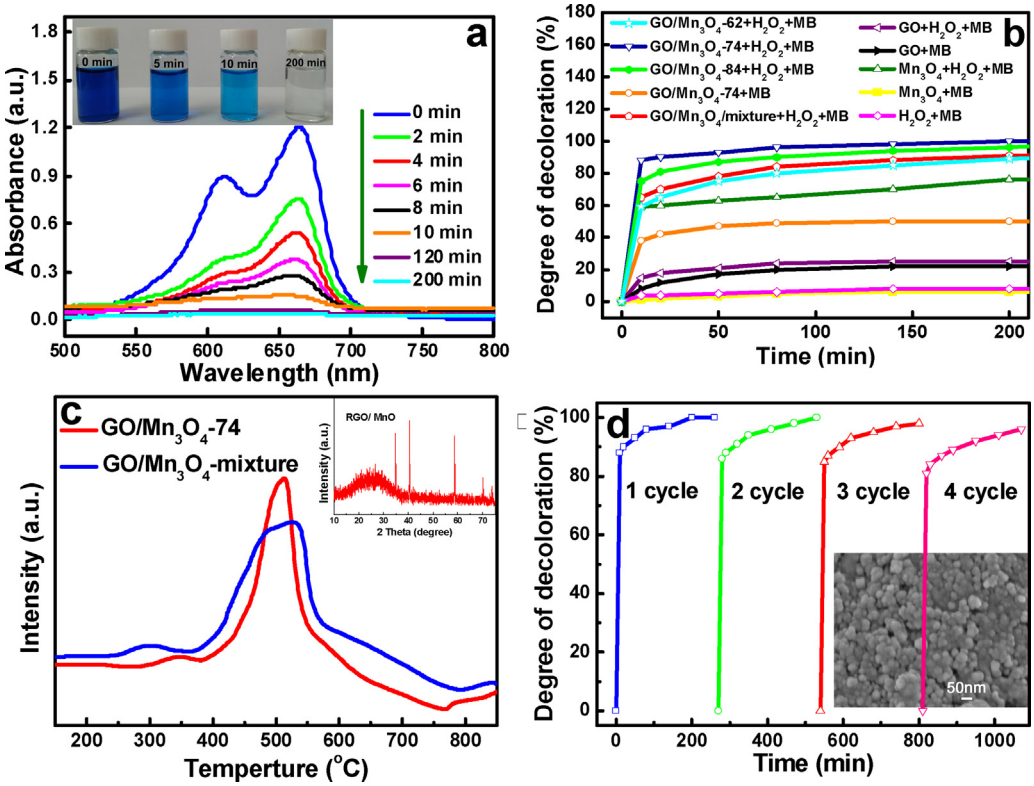

Fig. 6. (a) Absorption spectra of the MB solution (50 mg L^{-1}, 50 mL) in the presence of GO/Mn_3O_4-74 composite for the different time interval, inset is the photo image; (b) Time profiles of MB decolorization with the various samples under different condition; (c) H_2 TPR spectra of GO/Mn_3O_4-74 and GO/Mn_3O_4-mixture composites, inset is the final product of RGO/MnO after heat treatment; (d) Decolorization of MB with the recycled GO/Mn_3O_4-74 hybrid (reaction conditions: [MB] = 50 mg L^{-1}, [H_2O_2] = 10 mL, [catalyst] = 10 mg).

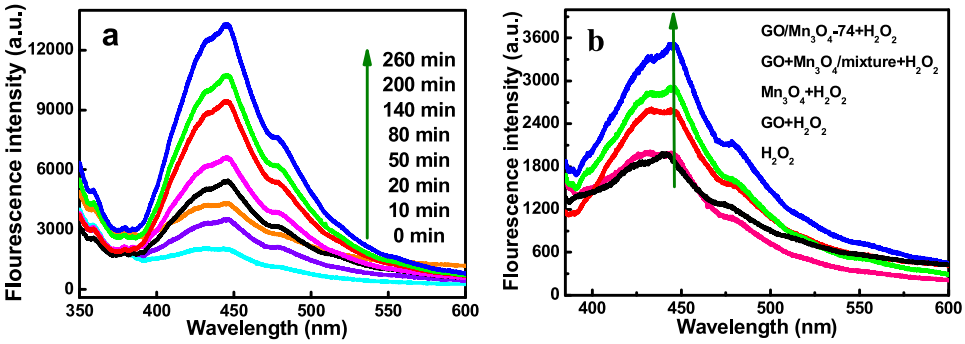

Fig. 7. (a) PL spectra changed with UV light irradiation time on GO/Mn_3O_4-74 composite in a 5×10^{-4} mol L^{-1} basic solution of TA (excitation at 325 nm) and (b) PL spectra of the various samples in a 5×10^{-4} mol L^{-1} basic solution of TA under UV light irradiation in a fixed 10 min.

to the O1s spectrum of GO/Mn_3O_4-74 composite (XPS datum in Fig. 3d), a large quantity of Mn—O—H bonds exist, which may come from oxygen-containing functional groups of GO [38] (Supporting information Fig. S1b). The experimental results also demonstrate that the MB decolorization for GO/Mn_3O_4-74 composite is much higher than that of GO/Mn_3O_4-mixture composite. Apparently, the chemical interactions between GO and Mn_3O_4 for GO/Mn_3O_4-74 composite are ought to play an essential role in the synergistic effect. H_2-TPR study of the obtained samples offers further evidence to prove the presence of above synergistic effect [41,42]. As shown in Fig. 6c, the actual TPR patterns were obtained by linearly increasing the temperature from room temperature to 850 °C. For GO/Mn_3O_4-74 composite, major H_2 consumption peaks locate at *ca.* 350 °C and 450–550 °C for GO/Mn_3O_4-74 composite, while the respective peaks are observed at 300 °C and 350–600 °C for GO/Mn_3O_4-mixture composite. Two peaks located at low and high temperature for both samples are, respectively, assigned to the reduction of GO into RGO and Mn_3O_4 into MnO (JCPDS no. 07-0230) (XRD pattern shown in inset of Fig. 6c). The temperature at which specific species is reduced from the surface indicates the higher the temperature, the stronger the surface bond [43]. Apparently, the as-prepared GO/Mn_3O_4-74 is much more stable during the H_2-TPR process compared with the GO/Mn_3O_4-mixture composite. This observation suggests the strong chemical interactions between GO and Mn_3O_4 in GO/Mn_3O_4-74 as well as small sizes of Mn_3O_4 particles.

The stability and recyclability of GO/Mn_3O_4-74 hybrid were evaluated by successive tests of MB decolorization, as shown in Fig. 6d. It is found that GO/Mn_3O_4-74 catalyst can work at least four cycles without any noticeable loss of catalytic activities, demonstrating the long-term durability of GO/Mn_3O_4-74 hybrid. To explain its good catalytic performance, GO/Mn_3O_4-74 hybrid reclaimed from catalytic tests is well studied (Fig. 6d). As shown in SEM image (inset image of Fig. 6d), Mn_3O_4 particles on the surfaces of GO exhibit similar size and morphology as those of the starting ones. XRD patterns and corresponding XPS spectra of the sample still remain unchanged after decolorization reaction of MB (Figs. 2a and 3c and d). Above results suggest that the structure of GO/Mn_3O_4-74 hybrid is stable during the catalytic reaction, which is attributed to the strong interaction between GO and Mn_3O_4. In order to identify such interaction, the Mn_3O_4 content leached from GO/Mn_3O_4-74 composite is tested by ICP [12]. The result shows that the final percentage of Mn_3O_4 lost from GO/Mn_3O_4-74 composite is about 0.4%. Therefore, GO/Mn_3O_4-74 hybrid has an excellent long-term stability and can be reused without noticeable loss of catalytic activity for decolorization of MB in water.

It is known that the main product of MB mineralization is SO_4^{2-}, and it is widely used to evaluate the efficiency of the catalytic degradation of MB [44]. The SO_4^{2-} ion concentration in the solution was determined by ion chromatography. The calculated concentration of SO_4^{2-} is 10.7 mg L^{-1} after 100% decolorization of MB for GO/Mn_3O_4-74 hybrid, while the measured concentration of SO_4^{2-} in the final solution is 8.7 mg L^{-1} (0.5 mg L^{-1} of sulfate comes from the H_2O_2 reagent). These results indicate that MB can be completely decolorized and nearly 77% mineralized over GO/Mn_3O_4-74 composite. The mineralization of 77% reported herein is much higher than that of our previously reported RGO/MnO_2 (66%) [12] and manganese oxide (27%) [44].

The catalytic activity of the prepared samples was further confirmed by the detection of •OH by a PL technique using TA as a probe molecule [45]. Fig. 7a shows the changes of PL spectra of TA solution under UV light irradiation with irradiation time. A gradual increase in PL intensity at about 445 nm is observed with time for GO/Mn_3O_4-74 composite, which suggests that the fluorescence comes from the chemical reactions between TA and •OH produced during catalytic reactions [44,46]. It is obvious that PL intensity is proportional to the amount of produced hydroxyl radicals. Fig. 7b shows the comparison of PL intensity for different samples illumined at a fixed time (10 min) with pure H_2O_2 as the reference. The amount of •OH produced on the tested samples decreases in the following order: GO/Mn_3O_4-74 > GO/Mn_3O_4-mixture > Mn_3O_4 > GO, which well agrees with their catalytic activity for MB decolorization as described in Fig. 6b. Our hydroxyl radical experiments further confirm that •OH species has a positive relation with the catalytic activity for degradation of MB in this study.

Some studies on oxidative degradation of organic dyes with H_2O_2 have been reported previously [44,46]. However, the exact mechanism for dye decomposition with H_2O_2 remains unclear. The superior performance of GO/Mn_3O_4 in the decomposition of MB could be attributed to the positive synergistic effect of GO, MB and Mn_3O_4 with the assistance of H_2O_2, as shown in Fig. 8. First, cationic MB molecules are easily adsorbed to the surfaces of GO by two approaches: electrostatic attraction as well as π–π conjugation based on the negatively charged structure and part π-conjugation system of GO. Such adsorption increases the effective concentration of MB molecules significantly near the surfaces of the GO/Mn_3O_4 composite, resulting in the highly catalytic decomposition rate. Second, the hydrophilic nature of GO leads to the well dispersion of GO/Mn_3O_4 composite in water, thus improve the wettability of the catalyst in aqueous solution. Third, excellent contact between Mn_3O_4 nanoparticles and GO sheets also prevent Mn_3O_4 from leaching out in the catalytic reactions, then efficiently catalyzing H_2O_2 to generate free •OH radical species and eventually facilitate the degradation of MB molecules. Fourth, some small molecules such as CO_2, H_2O and SO_4^{2-} *etc.* from the MB dye decomposition are desorbed from the Mn_3O_4 surface and the catalyst is recovered. Therefore, there would be a coupling between adsorption and catalytic reaction in a single process for GO/Mn_3O_4

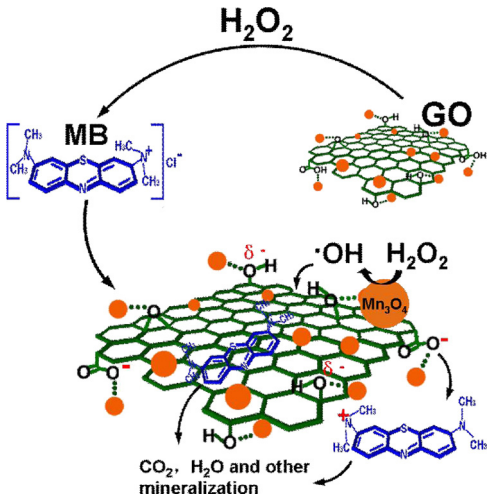

Fig. 8. Schematic illustration of MB decomposition on GO/Mn_3O_4 composite with the assistance of H_2O_2.

composite, resulting in an appreciable improvement in decomposition of MB compared with bare Mn_3O_4 and GO.

4. Conclusions

GO/Mn_3O_4 composites have been effectively fabricated with pristine GO/$MnSO_4$ suspension produced by the modified Hummers method as the raw materials. This atom-economic synthesis produces only K_2SO_4 crystal as the by-product, and avoids fussy procedure for the separation of GO from the GO/$MnSO_4$ suspension. The obtained GO/Mn_3O_4 composites have exhibited a good performance for decolorization of MB with the assistance of H_2O_2, and their high catalytic performance is mainly attributed to the synergistic effects of GO, Mn_3O_4 and MB molecules. It is found that negatively charged GO can effectively adsorb cationic MB molecules and its hydrophilic nature can improve the wettability of the catalyst to facilitate the decomposition of MB dye in water. Furthermore, excellent contact between Mn_3O_4 nanoparticles and GO sheets also prevent Mn_3O_4 from leaching out in the catalytic reactions, then efficiently catalyzing H_2O_2 to generate free •OH radical species for the degradation of MB molecules. The present research provides a green approach for synthesis of GO/Mn_3O_4 composites which show a promising candidate as the catalyst for the decomposition of organic compounds in water.

Acknowledgements

This work was supported by China Postdoctoral Science Foundation (2013M530922, 2014T70253), Program for Liaoning Excellent Talents in University (LJQ2014063, LJQ2013109) and Dalian Science and Technology Fund Plan (2013J21DW026).

Appendix A. Supplementary data

Supplementary material related to this article can be found, in the online version, at http://dx.doi.org/10.1016/j.apcatb.2014.06.058.

References

[1] R.J. Zou, Z.Y. Zhang, L. Yu, Q.W. Tian, Z.G. Chen, J.Q. Hu, Chem. Eur. J. 17 (2011) 13912–13917.
[2] Z.C. Bai, B. Sun, N. Fan, Z.C. Ju, M.H. Li, L.Q. Xu, Y.T. Qian, Chem. Eur. J. 18 (2012) 5319–5324.
[3] E. Rezaei, J. Soltan, Appl. Catal., B: Environ. 148–149 (2014) 70–79.
[4] Y. Gogotsi, J. Phys. Chem. Lett. 2 (2011) 2509–2510.
[5] S. Chowdhury, R. Balasubramanian, Appl. Catal., B: Environ. 160–161 (2014) 307–324.
[6] H. Hu, Z.B.Z., W.B. Wan, Y. Gogotsi, J.S. Qiu, Adv. Mater. 25 (2013) 2105–2245.
[7] M. Seredych, T.J. Bandosz, J. Mater. Chem. 22 (2012) 23525–23533.
[8] J.Y. Zhu, J.H. He, ACS Appl. Mater. Interfaces 4 (2012) 1770–1776.
[9] M. Seredych, T.J. Bandosz, Microporous Mesoporous Mater. 150 (2012) 55–63.
[10] H.Q. Sun, S.Z. Liu, G.L. Zhou, H.M. Ang, M.O. Tade, S.B. Wang, ACS Appl. Mater. Interfaces 4 (2012) 5466–5471.
[11] Y.J. Yao, C. Xu, S.M. Yu, D.W. Zhang, S.B. Wang, Ind. Eng. Chem. Res. 52 (2013) 3637–3645.
[12] J. Qu, L. Shi, C. He, F. Gao, B. Li, Q. Zhou, H. Hu, G. Shao, X. Wang, J. Qiu, Carbon 66 (2014) 485–492.
[13] D. Li, M.B. Muller, S. Gilje, R.B. Kaner, G.G. Wallace, Nat. Nanotechnol. 3 (2008) 101–105.
[14] X.W. Yang, J.W. Zhu, L. Qiu, D. Li, Adv. Mater. 23 (2011) 2833–2838.
[15] G.K. Ramesha, A.V. Kumara, H.B. Muralidhara, S. Sampath, J. Colloid Interface Sci. 361 (2011) 270–277.
[16] S. Chen, J.W. Zhu, X.D. Wu, Q.F. Han, X. Wang, ACS Nano 4 (2010) 2822–2830.
[17] P. Gao, D.D. Sun, Appl. Catal., B: Environ. 147 (2014) 888–896.
[18] S. Morales-Torres, L.M. Pastrana-Martinez, J.L. Figueiredo, J.L. Faria, A.M.T. Silva, Appl. Surf. Sci. 275 (2013) 361–368.
[19] R.F. Nie, J.J. Shi, S.X. Xia, L. Shen, P. Chen, Z.Y. Hou, F.S. Xiao, J. Mater. Chem. 22 (2012) 18115–18118.
[20] P. Gao, J.C. Liu, D.D. Sun, W. Ng, J. Hazard. Mater. 250 (2013) 412–420.
[21] Y.L. Min, K. Zhang, W. Zhao, F.C. Zheng, Y.C. Chen, Y.G. Zhang, Chem. Eng. J. 193 (2012) 203–210.
[22] G. Park, L. Bartolome, K.G. Lee, S.J. Lee, D.H. Kim, T.J. Park, Nanoscale 4 (2012) 3879–3885.
[23] X. Yang, C.L. Chen, J.X. Li, G.X. Zhao, X.M. Ren, X.K. Wang, RSC Adv. 2 (2012) 8821–8826.
[24] N.S. Andryushina, O.L. Stroyuk, Appl. Catal., B: Environ. 27 (2014) 148–149.
[25] Y.Y. Gao, X.P. Pu, D.F. Zhang, G.Q. Ding, X. Shao, J. Ma, Carbon 50 (2012) 4093–4101.
[26] J.C. Liu, L. Liu, H.W. Bai, Y.J. Wang, D.D. Sun, Appl. Catal., B: Environ. 106 (2011) 76–82.
[27] P.H. Shi, R.J. Su, F.Z. Wan, M.C. Zhu, D.X. Li, S.H. Xu, Appl. Catal., B: Environ. 123 (2012) 265–272.
[28] J.Y. Qu, G. Feng, Q. Zhou, Z.Y. Wang, H. Hu, B.B. Li, W.B. Wan, X.Z. Wang, J.S. Qiu, Nanoscale 5 (2013) 2999–3005.
[29] J. Yu, B. Wang, Appl. Catal., B: Environ. 94 (2010) 295–302.
[30] Z. Zheng, B. Huang, J. Lu, X. Qin, X. Zhang, Y. Dai, Chem. Eur. J. 17 (2011) 15032–15038.
[31] L. Wang, Y. Li, Z. Han, L. Chen, B. Qian, X. Jiang, J. Pinto, G. Yang, J. Mater. Chem. A: Mater. Energy Sustainability 1 (2013) 8385–8397.
[32] J.W. Lee, A.S. Hall, J.D. Kim, T.E. Mallouk, Chem. Mater. 24 (2012) 1158–1164.
[33] N. Li, Z. Geng, M. Cao, L. Ren, X. Zhao, B. Liu, Y. Tian, C. Hu, Carbon 54 (2013) 124–132.
[34] Y.Z. Wu, S.Q. Liu, H.Y. Wang, X.W. Wang, X. Zhang, G.H. Jin, Electrochim. Acta 90 (2013) 210–218.
[35] Z.Y. Wang, D.Y. Luan, S. Madhavi, Y. Hu, X.W. Lou, Energ. Environ. Sci. 5 (2012) 5252–5256.
[36] S. Chen, J. Zhu, X. Wu, Q. Han, X. Wang, ACS Nano 4 (2010) 2822–2830.
[37] X. Zhao, L.L. Zhang, S. Murali, M.D. Stoller, Q.H. Zhang, Y.W. Zhu, R.S. Ruoff, ACS Nano 6 (2012) 5404–5412.
[38] Y. Yao, C. Xu, S. Yu, D. Zhang, S. Wang, Ind. Eng. Chem. Res. 52 (2013) 3637–3645.
[39] T. Gan, J.Y. Sun, K.J. Huang, L. Song, Y.M. Li, Sens. Actuators, B: Chem. 177 (2013) 412–418.
[40] H. Wang, L.F. Cui, Y. Yang, H.S. Casalongue, J.T. Robinson, Y. Liang, Y. Cui, H. Dai, J. Am. Chem. Soc. 132 (2010) 13978–13980.
[41] S.I.N. Ayuthaya, N. Mongkolsiri, N. Praserthdam, P.L. Silveston, Appl. Catal., B: Environ. 43 (2003) 1–12.
[42] C. TorreAbreu, M.F. Ribeiro, C. Henriques, G. Delahay, Appl. Catal., B: Environ. 12 (1997) 249–262.
[43] M. Boaro, M. Vicario, C. de Leitenburg, G. Dolcetti, A. Trovarelli, Catal. Today 77 (2003) 407–417.
[44] L.L. Zhang, Y.L. Nie, C. Hu, X.X. Hu, J. Hazard. Mater. 190 (2011) 780–785.
[45] J. Yu, W. Wang, B. Cheng, B.L. Su, J. Phys. Chem. C 113 (2009) 6743–6750.
[46] T. Rhadfi, J.Y. Piquemal, L. Sicard, F. Herbst, E. Briot, M. Benedetti, A. Atlamsani, Appl. Catal., A: Gen. 386 (2010) 132–139.